Synergistic Effect of Cell-Derived Extracellular Matrices and Topography on Osteogenesis of Mesenchymal Stem Cells

Yang, Liangliang; Ge, Lu; van Rijn, Patrick

Published in:
ACS Applied Materials & Interfaces

DOI:
10.1021/acsami.0c05012

Publication date:
2020

ACS APPLIED MATERIALS & INTERFACES

www.acsami.org

Research Article

Synergistic Effect of Cell-Derived Extracellular Matrices and Topography on Osteogenesis of Mesenchymal Stem Cells

Liangliang Yang,* Lu Ge, and Patrick van Rijn*

Cite This: https://dx.doi.org/10.1021/acsami.0c05012

Read Online

ACCESS | Metrics & More | Article Recommendations | Supporting Information

ABSTRACT: Cell-derived matrices (CDMs) are an interesting alternative to conventional sources of extracellular matrices (ECMs) as CDMs mimic the natural ECM composition better and are therefore attractive as a scaffolding material for regulating the functions of stem cells. Previous research on stem cell differentiation has demonstrated that both surface topography and CDMs have a significant influence. However, not much focus has been devoted to elucidating possible synergistic effects of CDMs and topography on osteogenic differentiation of human bone marrow-derived mesenchymal stem cells (hBM-MSCs). In this study, polydimethylsiloxane (PDMS)-based anisotropic topographies (wrinkles) with various topography dimensions were prepared and subsequently combined with native ECMs produced by human fibroblasts that remained on the surface topography after decellularization. The synergistic effect of CDMs combined with topography on osteogenic differentiation of hBM-MSCs was investigated. The results showed that substrates with specific topography dimensions, coated with aligned CDMs, dramatically enhanced the capacity of osteogenesis as investigated using immunofluorescence staining for identifying osteopontin (OPN) and mineralization. Furthermore, the hBM-MSCs on the substrates decorated with CDMs exhibited a higher percentage of (Yes-associated protein) YAP inside the nucleus, stronger cell contractility, and greater formation of focal adhesions, illustrating that enhanced osteogenesis is partly mediated by cellular tension and mechanotransduction following the YAP pathway. Taken together, our findings highlight the importance of ECMs mediating the osteogenic differentiation of stem cells, and the combination of CDMs and topography will be a powerful approach for material-driven osteogenesis.

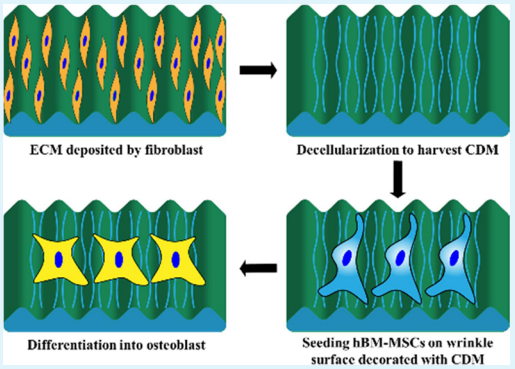

KEYWORDS: *extracellular matrix, topography, mesenchymal stem cells, osteogenic differentiation, mechanotransduction*

1. INTRODUCTION

In in vivo conditions, cells directly interact with their surrounding microenvironment, the extracellular matrix, which is secreted by cells and composed of a complex mixture of polysaccharides and proteins. The ECM provides mechanical support and further introduces many biochemical and biophysical stimuli, including adhesion receptors, topographical cues, and mechanical input for regulating cell responses, such as cell adhesion/spreading, proliferation, migration, differentiation, or apoptosis.[1] Therefore, mimicking the interactions of the natural ECM and incorporating such approaches in the development of biomaterials enable studying of cells in a realistic and adaptable cell microenvironment in vitro.[2,3]

For topography, considerable research has highlighted the essential role of substrate topography in the cell behavior and lineage commitment of different types of stem cells,[4,5] and this can be adjusted by the types and parameters of the topographical structures.[6−8] Furthermore, in vivo, there are many tissues composed of well-aligned and anisotropic architectures with nano- and microscale features (e.g., tendons, bones, and nerves); therefore, it is important to mimic the anisotropic structure of the bone ECM for biomaterials to study the influence on cell behaviors. Cells could sense surface parameters varying from 10 nm to 100 μm by contact guidance.[9,10] Previously, our group fabricated topography-containing surfaces and gradients with nano- and microscale features and found that topography parameters have a significant effect on cells, including cell adhesion, elongation, orientation, migration, and differentiation of stem cells.[11−17] The aligned topographies were envisioned to represent the ECM fiber morphology better, which is important as the fibrous structure of the cellular microenvironment in vivo is essential for directing numerous cell functions.[18] In recent years, cellular adhesion proteins/peptides have been applied as

Received: March 17, 2020
Accepted: May 19, 2020
Published: May 19, 2020

biomimicking matrices for improving the biocompatibility of biomaterials by chemical attachment or physisorption, e.g., ECM components (collagen[19] and fibronectin[20]), Matrigel,[21] GRGDS,[22] GYIGSR,[23] IKVAV,[24] N-cadherin,[25] and E-cadherin.[26] However, individual ECM proteins/peptides cannot completely mimic the complexity of the endogenous ECM and often lack powerful topographical stimuli. Therefore, diverse ECM proteins that mimic the composition of the ECM in vivo should be investigated to gain insights into how to further push the control of stem cell differentiation.

In recent years, there has been increasing interest in developing CDMs, derived from native tissues or cells cultured in vitro, to form a microenvironment that mimics a native niche.[27,28] The CDM represents best the cellular microenvironment in tissues.[29] The decellularized ECM is a noncellular component containing various cell-secreted macromolecules that provides a natural scaffold of similar biological and structural make-up. While the CDM may differ significantly depending on the origin (cell type and tissue), it mostly consists of proteoglycans, such as growth factors, glycosaminoglycans (GAGs), and matrix proteins, e.g., collagen (Col I), fibronectin (Fn), elastin, vitronectin, and laminin.[30] Previously, it has been demonstrated that biochemical and biophysical cues can be conserved after the removal of the cellular components while removing components such as DNA and cellular components that trigger immune responses,[31] which makes the decellularized ECM a (stem) cell substrate that is close to the natural environment.[27,32,33] CDMs could be generated from different cell sources, e.g., fibroblasts,[34,35] mesenchymal stem cells,[36,37] and pluripotent stem cells.[33] Compared to other cell types, human dermal fibroblasts have several advantages, for example, readily isolated, substantial secretion of ECM biomolecules,[38] and the matrices generated from fibroblasts are much stronger than those of collagen or fibrin gels, which are often the reconstituted ECM components of choice.[39] Leach et al.[32] found that cell-derived extracellular matrices from bone marrow-derived mesenchymal stem cells, human dermal fibroblasts, and adipose stromal cells all promote the osteogenic differentiation; therefore, human dermal fibroblasts are a highly interesting cell source that secretes substantial amounts of relevant ECMs.

Much work so far has focused on the influence of CDMs derived from cells on multilineage differentiation potential; for instance, Tuan and co-workers[40] showed that CDMs from mesenchymal stem cells (MSCs) dramatically enhanced attachment, proliferation, migration, and differentiation of MSCs (osteogenenic and adipogenic differentiation), as compared to surfaces coated with Col I. Furthermore, Li et al.[33] found that CDMs from aggregates of pluripotent stem cells modulate neurogenesis through biological cues and biophysical properties. These studies indicate that CDM scaffolds are interesting for tissue engineering with many possibilities in applications for tissue engineering and regenerative medicine. However, very few studies have been undertaken for investigating potential synergistic effects of topography and CDMs on stem cell osteogenesis.

In this study, we aim to explore the synergism of anisotropic topography and fibroblast-derived CDMs on the osteogenesis of hBM-MSCs. We hypothesized that the combination of topography and fibroblast-derived ECMs would significantly enhance the fate commitment toward osteogenesis of hBM-MSCs. For this purpose, PDMS-based anisotropic topographies varying in wavelengths and amplitudes were used, which were found to interact with hBM-MSCs in our previous work.[14] As shown in Figure 1, MSCs were seeded on topography substrates decorated with the fibroblast-derived ECM after decellularization and allowed to expand following the standard culture procedure. The presence of endogenous ECM proteins, Col I and Fn, were confirmed by immunofluorescence labeling. The degree of osteogenic differentiation of hBM-MSCs was analyzed using immunofluorescence labeling of OPN and mineralization by staining the mineral phase with Alizarin red. Furthermore, the formation of focal adhesions, cell contractility, and activation of the YAP signal pathway were analyzed in depth to reveal the mechanism of MSC responses to the wrinkle substrates decorated with CDMs. We found that substrates decorated with CDMs had a remarkable effect on cell orientation and cell area and that there is a synergistic effect of specific topography combined with CDMs on the osteogenic differentiation of hBM-MSCs, probably mediated by the focal adhesion, cytoskeletal contractility, and YAP signaling pathway.

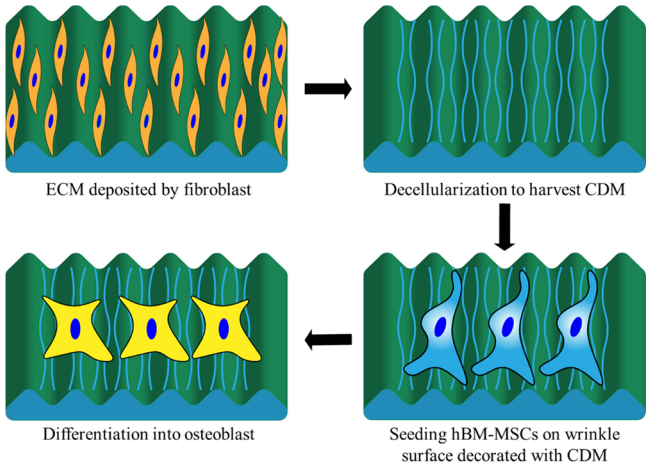

Figure 1. Schematic representation of the preparation process of the CDM. Fibroblast-derived extracellular matrices were obtained through a decellularization process of cultured fibroblasts. Then, onto the matrix, hBM-MSCs were seeded to investigate the co-effect of topography and CDMs on osteogenesis.

2. METHODS

2.1. PDMS Substrate Preparation. PDMS substrates were prepared as described previously.[14] Briefly, PDMS was prepared by combining an elastomer prepolymer and a cross-linking agent (Sylgard 184, Dow Corning) in a ratio of 10:1 by weight, and the mixture was degassed for 15 min to remove air. The PDMS was subsequently further cured at 70 °C overnight.

2.2. Preparation of PDMS-Aligned Topography Substrates (Molds). PDMS substrates with aligned wrinkle topography were prepared as previously reported.[14] The PDMS elastomeric substrate was uniaxially stretched to 120−130% of the initial length and subsequently oxidized with air plasma (Plasma Activate Flecto 10 USB, maximum intensity) using different pressures and variations in time depending on the desired features. Afterward, the strain was released, and an anisotropic wrinkle with various wavelengths and amplitudes was formed. Table 1 summarizes the conditions for wrinkle substrate preparations. The samples prepared in this step were used as the molds for imprinting.

2.3. Imprinting. To exclude chemical and mechanical variations originating from the different preparation procedures, a mixture of prepolymers and cross-linking agents (ratio of 10:1, weight) was poured onto the surface of the wrinkle substrates acting as the mold,

https://dx.doi.org/10.1021/acsami.0c05012
ACS Appl. Mater. Interfaces XXXX, XXX, XXX−XXX

Table 1. Conditions for Wrinkle Preparation on PDMS Substrates Used for Molds[a]

substrate	ratio of prepolymer and curing agent	stretched percentage (%)	operating pressure (Torr)	plasma time (s)
W0.5/ A0.05	10:1	30	14	60
W3/ A0.7	10:1	30	0.025	20
W10/ A3.5	10:1	20	0.025	650

[a]W and A represent the wavelength and amplitude, respectively, and are expressed in μm. The substrates were further indicated as W0.5, W3, and W10.

prepared in the last step, and was cured at 70 °C overnight. Afterward, the freshly prepared substrates were detached from the mold and treated with air plasma before cell seeding at 500 mTorr for 1 min. The Flat control sample was treated similar to the imprints indicated above (10:1 for the prepolymer and the cross-linking agent; the same curing and oxidization process), to guarantee that the substrates retain similar surface physicochemical properties.

2.4. Topography Characterization. Topography was characterized using an atomic force microscope (AFM, Nanoscope V Dimension 3100 microscope, Veeco, United States) using a tapping mode approach in air (DNP-10 tip). The features were analyzed using NanoScope Analysis software.

2.5. Fibroblast-Derived Extracellular Matrix Formation. Substrates bearing decellularized ECMs were prepared similarly to previously reported with modifications.[38,41] Briefly, human dermal fibroblasts were seeded at a density of 2×10^4 cells/well in 24-well plates containing different PDMS substrates (Flat and topography) and cultured in RPMI-1640 supplemented with 10% fetal bovine serum (Gibco), 1% penicillin/streptomycin (Gibco), 0.1% ascorbic acid 2-phosphate (Sigma), and 1% glutamax (Gibco). Every 3 days, the medium was refreshed. A confluent cell layer reached after 10 days and was washed with phosphate-buffered saline (PBS) twice and subsequently decellularized upon incubation with a 0.5% Triton X-100 solution and 20 mM NH_4OH in PBS at 37 °C for 10 min. The samples were afterward treated with a 10 μg/mL solution of DNase I (Roche) at 37 °C for 2 h to get rid of any DNA contamination. The decellularized CDM was gently washed with PBS five times to completely remove all of the sacrificial fibroblasts, and the resulting CDM was immediately used or kept under sterile conditions at 4 °C before use.

2.6. Cell Culture. hBM-MSCs from Lonza (passage 2) were cultured in a growth medium supplemented with Alpha modified Eagle's medium (Gibco), 10% fetal bovine serum (Gibco), 0.1% ascorbic acid 2-phosphate (Sigma), and 1% penicillin/streptomycin (Gibco). Cells were incubated at 37 °C with 5% CO_2. Every 3 days, the culture medium was refreshed, and cells were passaged or harvested at approximately 80% confluence. The confluent cells were subcultured by trypsinization. hBM-MSCs of passage 4 were used for the next experiments.

2.7. Immunostaining. PDMS substrates were washed with 70% ethanol for sterilization and put in 24-well plates. The substrates were washed with PBS prior to use. Afterward, hBM-MSCs were seeded at a density of 1×10^4 cells/well. For immunostaining, hBM-MSCs were rinsed with Dulbecco's PBS (DPBS) and subsequently fixed using 3.7% paraformaldehyde (PFA) solution in PBS for 20 min. Afterward, the membrane of the cell was permeabilized using a 0.5% Triton X-

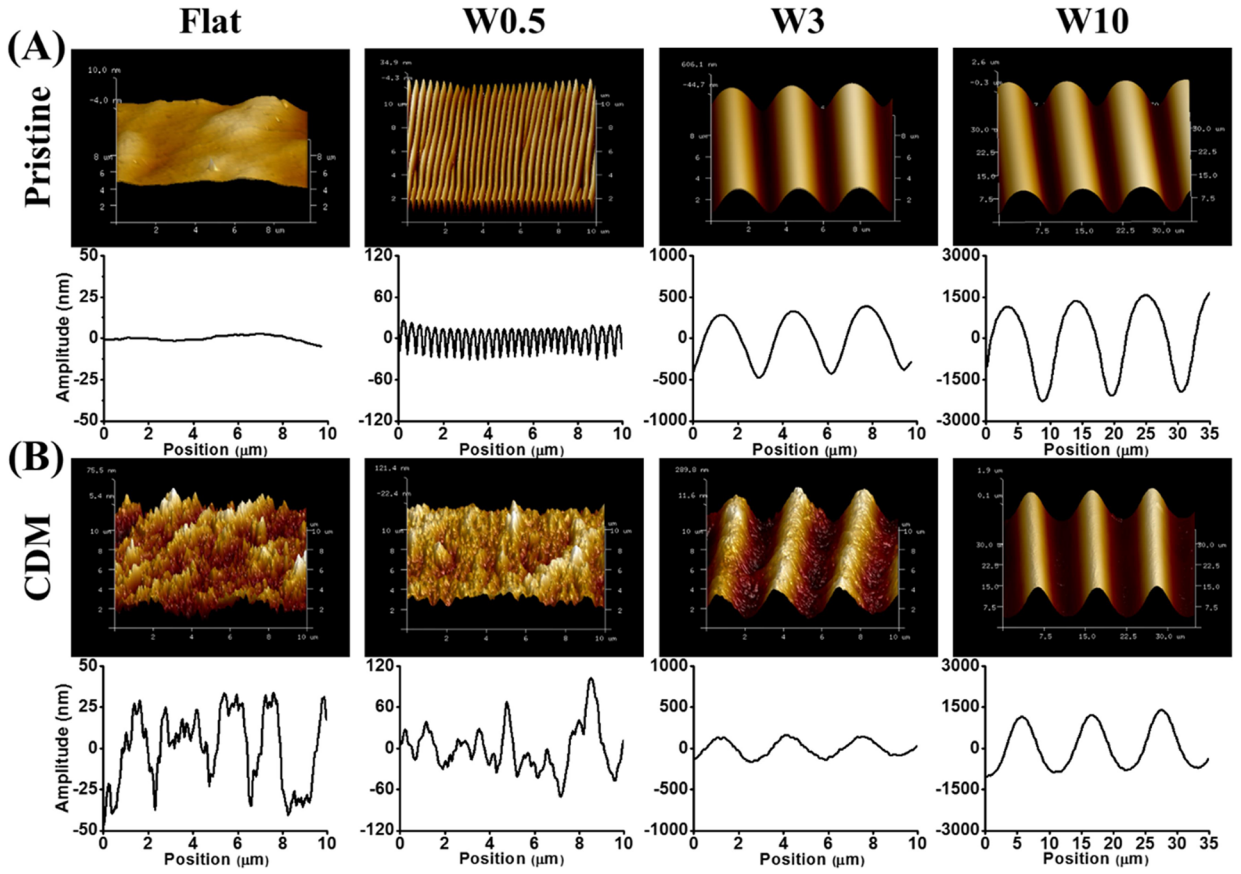

Figure 2. Representative AFM images of the substrate and topography profiles (height) of the structured PDMS substrates obtained (A) after imprinting and (B) after ECM deposition by fibroblasts with subsequent decellularization. W0.5, W3, and W10 stand for W0.5/A0.05, W3/A0.7, and W10/A3.5, respectively, and W is the abbreviation of wavelength.

https://dx.doi.org/10.1021/acsami.0c05012
ACS Appl. Mater. Interfaces XXXX, XXX, XXX−XXX

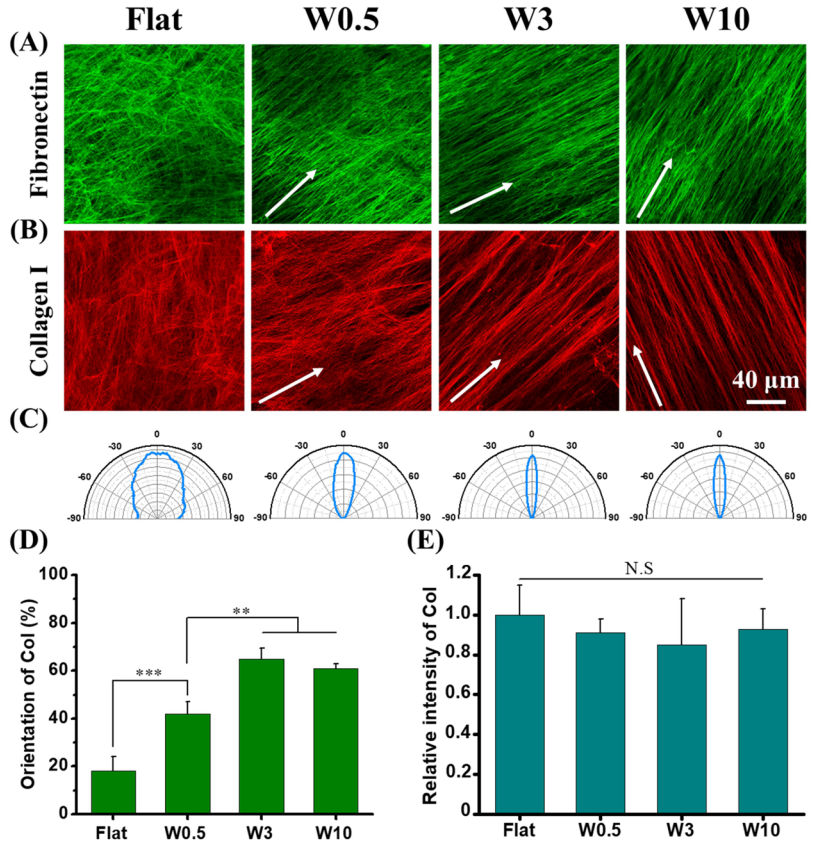

Figure 3. Representative immunofluorescence image of macromolecular ECM components (A: Fn; B: Col I) after decellularization. The white color arrows refer to the direction of the wrinkle. The scale bar is 40 μm. (C) Corresponding angular graph of the Col I orientation on different substrates, (D) statistical analysis of the Col I orientation, and (E) quantified fluorescence intensity of Col I compared to the mean values of the Flat substrate. Five images for each substrate were analyzed. Data are shown as mean ± standard deviation (SD), and N.S represents not significant, and $^{**}P < 0.01$, $^{***}P < 0.001$.

100 solution for 3 min and blocked with 5% bovine serum albumin (BSA) in PBS solution for 30 min. The cells were subsequently incubated with a primary antibody for collagen (Sigma, 1:100), fibronectin (Sigma, 1:100), OPN (Developmental Hybridoma Bank, MPIIIB10, 1:100), vinculin (clone hVin-1, Sigma, 1:100), phosphorylated myosin light chains (pMLCs, Cell Signaling, #3675, 1:200), and YAP (Santa Cruz Biotechnology, SC-101199, 1:100) for 1 h followed by treatment with a secondary antibody, Rhodamine Red-X-labeled goat-anti-mouse antibody (Jackson Immunolab, 1:100). Finally, the nucleus and cytoskeleton were stained with DAPI and FITC/TRITC-phalloidin, respectively, upon incubation for another 1 h. For imaging of the cells, a TissueFaxs microscope (TissueGnostics GmbH, Vienna, Austria) was used. Vinculin, pMLC, and YAP staining procedures were performed using a LEICA TCS SP2 confocal laser scanning microscope (CLSM) equipped with a 40× NA 0.80 water immersion objective. Additionally, focal adhesion determinations were performed by analysis of the images using an online Focal Adhesion Analysis Server,[42] and elongation of focal adhesion was said to be the ratio between the length of the major axis to the width of the minor axis; thereby, the cell with a perfect circle shape has an elongation of 1 (also applied for cell elongation). The myosin fluorescence intensity was determined as previously reported.[43]

2.8. Osteogenic Differentiation of hBM-MSCs. hBM-MSCs were cultured on the different samples at a cell density of 1×10^4 cells/well in 24-well plates. Cells were incubated at 37 °C with 5% CO_2, and after 24 h, the growth medium was exchanged for the osteogenic induction medium (OM), which was composed of a growth medium supplemented with 10 mM glycerophosphate (Sigma) and 100 nM dexamethasone (Sigma). The cells were cultured over a period of 14−21 days, and replacement of the medium was done every 3 days.

2.9. Mineralization Identification by Alizarin Red Staining. The mineralization of the ECM was analyzed by Alizarin Red staining after culturing the cells for 21 days under differentiation conditions. The samples were washed with PBS twice, fixed with 4% PFA for 15 min, and incubated with 0.1% Alizarin Red solution at room temperature for 30 min. Cells were washed with PBS two times before imaging. For quantification of the mineralization, the stained nodules were extracted for 30 min with 10% cetylpyridinum chloride in 10 mM sodium phosphate buffer at room temperature. The absorbance was determined using a microplate reader (BMG LABTECH, Offenburg, Germany) at 540 nm to determine quantitatively the amount of stain present. Normalization was performed for the results by accounting for the cell number in each well. The number of cells was calculated by quantitative analysis of DAPI positive nuclei using TissueQuest software after imaging with a TissueFaxs-Tissue-Gnostics microscopy setup in a high-throughput manner.

2.10. Statistics. Data are given as mean values ± standard deviation (SD). Origin 9.0 software was used for statistical analysis. One way analysis of variance (ANOVA) with Tukey's test was used for all data to determine differences between groups. $^{*}P < 0.05$, $^{**}P < 0.01$, and $^{***}P < 0.001$.

3. RESULTS

3.1. Topography-CDM Substrate Fabrication and Characterization. To determine the synergism between topography and CDMs on the differentiation behavior of stem cells, CDMs were prepared by cultivating fibroblasts on the substrates with different aligned topographies for 10 days,

https://dx.doi.org/10.1021/acsami.0c05012
ACS Appl. Mater. Interfaces XXXX, XXX, XXX−XXX

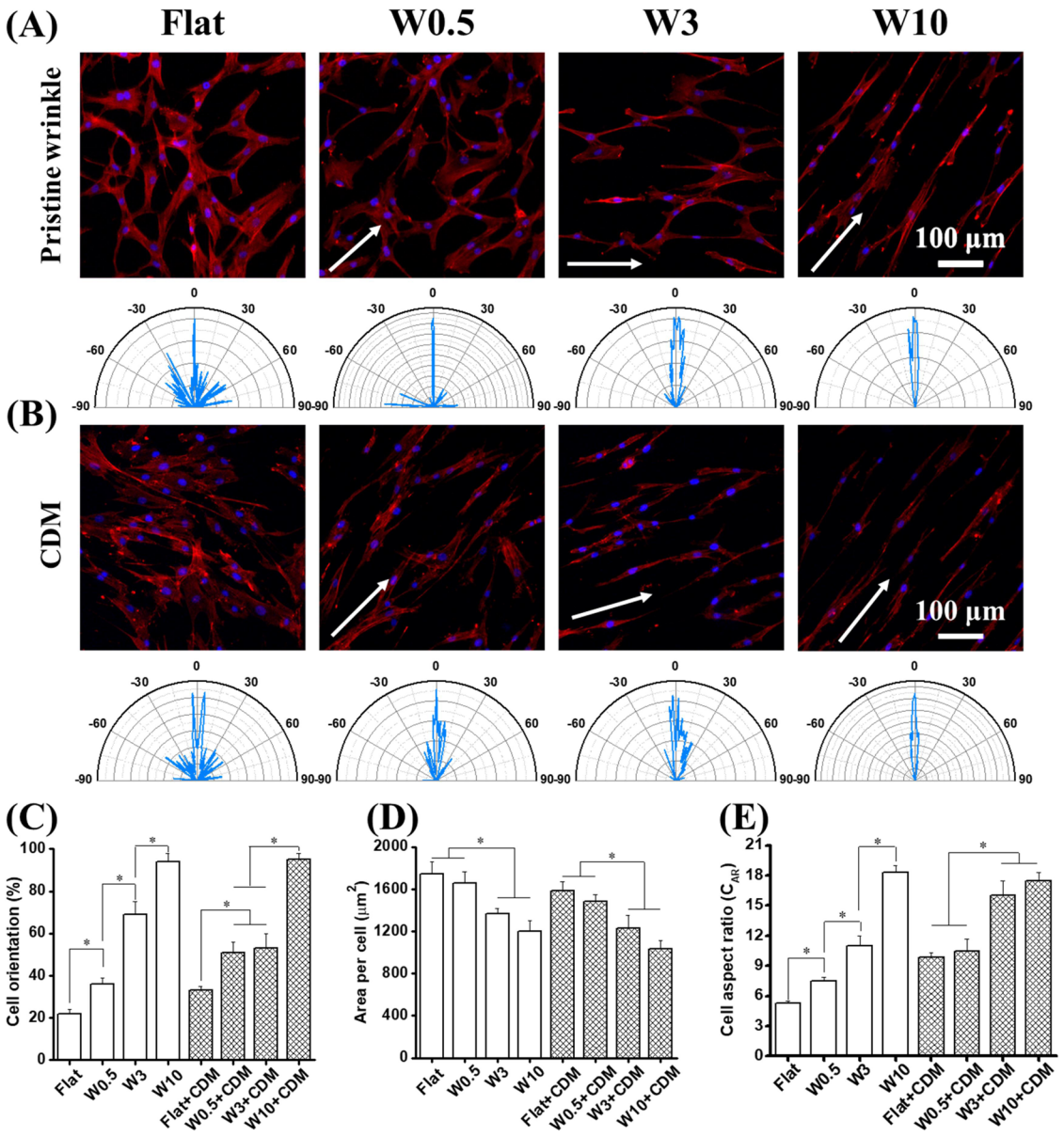

Figure 4. Representative fluorescence microscopy images of hBM-MSCs grown on (A) pristine topography and (B) substrates deposited with the CDM for 1 day, respectively. The row below the fluorescence image shows the corresponding angular graph of the cell cytoskeleton orientation on different substrates. The cytoskeleton (red) and the nucleus (blue) were visualized using TRITC-labeled phalloidin and DAPI as stains, respectively. The arrow represents the direction of the wrinkle. The scale bar is 100 μm for all the images. Statistical analysis of (C) cell orientation, (D) area per cell, and (E) cell aspect ratio ($n \geq 60$ cells, three independent experiments). Data are shown as mean ± standard deviation (SD), and $^*P < 0.05$.

which were subsequently decellularized using a chemical approach.

In this study, PDMS substrates with aligned topographies were prepared as described previously.[14,15] The topographies after imprinting were determined and visualized by AFM. As shown in Figure 2A, based on the preparation conditions as shown in Table 1, wrinklelike topographies were fabricated with different wavelengths (W; μm) and amplitudes (A; μm). For the wrinkle substrate, the anisotropic wavelike structure could be clearly observed. The amplitude increased with increasing wavelength; both these features were coupled and associated with the degree of oxidation of the surface, i.e., the time of plasma oxidation treatment. The amplitudes of the topography were 0.05, 0.7, and 3.5 μm for W0.5, W3, and W10, respectively. The different substrates with the aligned topographies are denoted as W0.5, W3, and W10. Flat was used as the control.

After the fibroblast culture and subsequent decellularization, the remaining CDMs had a significant influence on the surface topography of the substrate (Figure 2B). For Flat, compared to the smooth surface before CDM deposition (original), the surface with CDMs showed a much rougher surface structure, indicating the presence of a newly added layer. For W0.5, intriguingly, the CDM completely covered the original wavelike structure, which could no longer be observed. For W3, the topography was still clearly distinguishable after CDM deposition although the amplitude decreased from 0.7 to about 0.4 μm, indicating that more CDMs were collected at the bottom of the wavelike structure. The change in roughness was not clear on the W10 substrate, which may be due to the larger

https://dx.doi.org/10.1021/acsami.0c05012
ACS Appl. Mater. Interfaces XXXX, XXX, XXX−XXX

dimension, but here also the amplitude decreased substantially from 3.5 to about 2.2 μm.

To further confirm that the visualized layer on top of the substrates using AFM was indeed the decellularized ECM, two major ECM glycoproteins (Fn and Col I) were stained by immunofluorescence. Both proteins were found to be present in the CDM, suggesting the maintenance of bioactivity in the fibroblast-derived ECM. As illustrated in Figure 3, the ECM proteins displayed an anisotropic structure (along the direction of the wrinkle) on all the substrates except Flat, which showed isotropic fiber structures. Upon increasing wrinkle size, the orientation degree of Fn (Figure 3A) and Col I (Figure 3B) increased. Furthermore, the ECM proteins were organized into a network, indicating that CDM organization and structure were well retained after decellularization.

To further confirm the discrepancy between different substrates, the orientation distribution of the Col I fiber was measured (Figure 3C). Compared with the broad orientation distribution of Col I for Flat and W0.5, there was a narrow distribution for W3 and W10, indicating the higher level of orientation. We also quantitatively analyzed the orientation of Col I, calculated as the percentage of the main axis of the fiber within 10° from the direction of topography.[44,45] As shown in Figure 3D, W3 and W10 displayed the highest degree of orientation (65 and 61%, respectively), much higher than that for W0.5 (42%). The Flat control displayed no specific orientation, which is to be expected as there is no surface structuring present. Furthermore, the fluorescence intensity for Col I (Figure 3E) and Fn (Figure S3), major components in the ECM, was quantified by Fiji. The results showed that no significant difference was found for the various samples, suggesting that the amount of deposited CDM was similar on all substrates. These results demonstrate that the CDM maintains the proper morphology after decellularization and that substrate topography has a noteworthy influence on the orientation of deposited Fn and Col I in the CDM. The orientation of the CDM most likely results from the initial orientation of the cultured fibroblast that also responded well to the W3 and W10 anisotropic structures (Figure S1).

3.2. hBM-MSC Morphology on CDM-Deposited Topography Substrates. Morphology and structures, such as cell area and cell orientation, are important factors in the function of native tissues and organs on both biological and mechanical levels.[46] For identifying the influence of the deposited CDM on the morphology of the cells, hBM-MSCs were cultured on pristine topography and the substrates coated with the CDM after decellularization and allowed to adhere and attach/spread for 1 day. To analyze the cell nucleus and cytoskeleton, cells were stained with DAPI and phalloidin, respectively. Cell orientation, calculated as the percentage of the cells that have their main axis within 10° of the topography direction,[44,45] was determined using Fiji.

As illustrated in Figure 4A,B, the orientation of hBM-MSCs was highly influenced by the topography and the CDM. Fibroblasts grown on the different substrates were also stained after culturing for 1 and 10 days, which is shown in Figure S1. The highly oriented fibroblasts resemble also the high-degree CDM alignment. Apparently, the deposited CDM follows the orientation of the cells. For the pristine substrates of Flat and W0.5 without a CDM coating, hBM-MSCs were randomly oriented (the orientation degree was 22% (randomly chosen direction as there is no surface topography direction) and 36%, respectively, Figure 4C) after 1 day. In contrast, cells on W3 and W10 displayed a higher degree of orientation (69 and 94%, respectively) along the direction of the topography. For the substrates on which the deposited CDM resides, there is a slight increase in the orientation level for W0.5 + CDM (51%) compared to the pristine substrates, indicating that the CDM could facilitate the orientation of hBM-MSCs for the smaller wrinkle surface (W0.5). This indicates that even though the CDM layer covers the W0.5 topographies and is not identifiable anymore, the alignment of the fibroblasts still deposits the CDM in the direction of the wrinkles though it is less pronounced than that for the W3 and W10. The CDM then most likely acts as another topography substrate and guides the cell orientation with the anisotropic protein fibers of the CDM (as shown in Figure 3A,B). In contrast, the cell orientation decreased for W3 + CDM (53%), compared with W3, possibly due to the decreased amplitude after CDM deposition, which may diminish the response to the topography. However, there is no change in the orientation distribution for W10 and W10 + CDM.

The average single cell area (area/cell, μm^2) was also quantified as it is well known that cell adhesion and spreading are able to influence the expression of differentiation markers of stem cells.[47] As shown in Figure 4D, for pristine wrinkle substrates, the average area/cell gradually decreased with increasing wrinkle dimensions. The cell area was 1742, 1659, 1368, and 1202 μm^2 for Flat, W0.5, W3, and W10, respectively. Interestingly, the area/cell slightly decreased after CDM deposition. For Flat + CDM, W0.5 + CDM, W3 + CDM, and W10 + CDM, the cell area was about 1583, 1480, 1230, and 1030 μm^2, respectively. The reason for the decreasing cell area for each substrate, for instance, Flat versus Flat + CDM, may be attributed to the CDM deposition, increasing the roughness of the substrate where cells are grown and leading to the limitation of cell spreading. Furthermore, the density of hBM-MSCs was quantified for 1 and 14 days after seeding, and the results indicate that no significant difference was found for the pristine substrates compared to substrates coated with the CDM (Figure S2). The cell aspect ratio (C_{AR}) was also quantified (Figure 4E), and for cells cultured on W0.5, W3, and W10, the C_{AR} was 7.5, 11, and 18.3, respectively, much higher than that of cells grown on Flat (C_{AR} of 5.3). Intriguingly, substrates with the deposited CDM enhanced the cell elongation. C_{AR} for Flat + CDM, W0.5 + CDM, and W3 + CDM was 9.8, 10.5, and 16, respectively. However, there is not much difference for W10 versus W10 + CDM. Collectively, these findings elucidate the significant influence of the CDM, the native ECM, on the cell orientation, cell area, and cell elongation and show that the addition of CDMs does not automatically lead to more spreading.

3.3. Topography and CDMs Display a Synergistic Effect on MSC Osteogenesis. To determine the synergistic effect of topography and CDMs on osteogenesis of hBM-MSCs, these cells were cultured on the original wrinkle substrates and substrates bearing the CDM, respectively, and using the osteogenic induction medium (OM) as the culture medium for 14 days. After this, the cells were fluorescently labeled for osteopontin (OPN), a well-documented marker expressed in the later process of osteogenesis.[48] The cells stained using OPN were imaged by TissueFaxs, which is a high-throughput imaging method that provides the possibility of maintaining the same parameters during the whole imaging process allowing for the fluorescence output to be compared appropriately for quantification. As shown in Figure 5A, the

https://dx.doi.org/10.1021/acsami.0c05012
ACS Appl. Mater. Interfaces XXXX, XXX, XXX−XXX

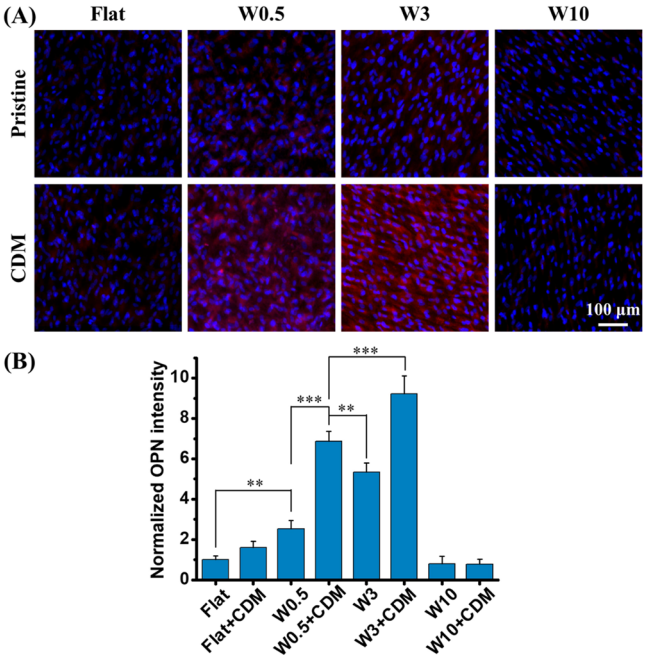

Figure 5. (A) Immunofluorescence labeling of the osteogenic marker OPN of hBM-MSCs cultured on the original substrate and CDM substrates cultured for 14 days in OM. hBM-MSCs were labeled for nuclei (DAPI, blue) and OPN (red). The scale bar is 100 μm for all images. (B) Quantification of OPN expression in the cells cultured in OM at day 14, normalized by the cell number ($n \geq 100$ cells, three independent experiments). Data are shown as mean ± standard deviation (SD), and $^{**}P < 0.01$, $^{***}P < 0.001$.

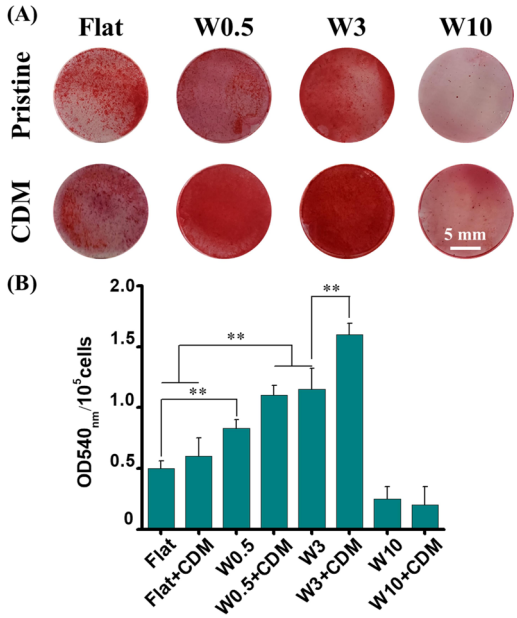

Figure 6. (A) Representative photographs of Alizarin Red-stained calcium nodules indicating extracellular calcium deposits by osteoblasts derived from hBM-MSCs cultured for 21 days in OM. (B) Mineralization quantification by elution of Alizarin Red S from the stained mineral bone matrix. Data are shown as mean ± standard deviation (SD), and $^{**}P < 0.01$. The scale bar is 5 mm.

cells grown on Flat and W10 compared to those on W0.5 and W3 exhibited a higher expression level of OPN. Interestingly, for the cells cultured on the substrates decorated with the CDM, the differentiation capacity was enhanced, especially for W0.5 and W3. In contrast, there was no prominent difference for Flat and W10 between pristine substrates and coated with the CDM. The effect was further quantified, and as shown in Figure 5B, the OPN level of cells on W0.5 + CDM and W3 + CDM was a 2.72-fold and 1.73-fold increase with respect to that on W0.5 and W3, respectively. In contrast, no significant difference was found between the group of Flat and Flat + CDM, W10 and W10 + CDM. These findings suggest that the CDM layer could significantly improve the differentiation toward the osteogenic lineage but not in a similar degree for all substrates, that only a specific topography is able to enhance the CDM effect, and that the CDM by itself only displays a minor contribution without the presence of topography as indicated by the comparison between Flat and Flat + CDM.

In order to further confirm the differentiation behavior, the cultures were treated with Alizarin red after culturing for 21 days, which is able to visualize calcium deposition, an important indicator to determine the final stage of osteogenic differentiation.[49] As shown in Figure 6A, the samples of Flat, W0.5, and W3 were positive for Alizarin red (red color); however, none of the cells cultured on W10 displayed mineral deposition. Interestingly, hBM-MSCs cultured on the substrate coated with the CDM showed more mineralized calcium nodules than pristine wrinkle surfaces. To quantify the mineralization of hBM-MSCs, calcium deposits were de-stained, and to determine the amount of extracted stain, the optical density (OD) was measured at 540 nm. As shown in Figure 6B, W3 + CDM displayed the highest OD_{540}, which points toward enhanced osteogenic differentiation capabilities. These results demonstrate that the CDM layer tremendously facilitates the mineralization secreted by hBM-MSCs but only for distinct substrates, and the added positive effects of the CDM differed much among the different substrates. The variations in the additive effects of the CDM and its amount indicate a synergistic effect for W0.5 and even more so for W3 as the increase is much higher than expected considering the contribution of the CDM on the Flat substrates and pristine W0.5 or W3.

3.4. Enhanced Osteogenesis of hBM-MSCs on Topography Decorated with CDM Mediated by Mechanotransduction. It is well documented that the fate of stem cells is regulated by physicochemical stimulation from the surrounding ECM via a process of mechanotransduction,[1] which transduces the physicochemical input into (bio)-chemical signals.[50] To obtain insights into potential signaling proteins involved in transduction of the physochemical stimuli, we investigated the localization expression of vinculin, Myosin, and YAP, all of which have been demonstrated to enhance osteogenic differentiation.[51−53] From the results of OPN expression and mineral production, the Flat, Flat + CDM, W3, and W3 + CDM were selected for further investigation.

The Hippo transcriptional coactivator Yes-associated protein (YAP) has recently been identified as a mechanical rheostat of the cell[54] and was shown to mediate osteogenic differentiation.[52,53] Phosphorylation induces the inactivation of YAP in the cytoplasm. Alternatively, the activated YAP is translocated into the nucleus, inducing the expression of genes involved in osteogenic differentiation. To investigate topography-induced YAP activation with and without CDMs, we immunostained for YAP and quantified the fraction localized to the nucleus of the hBM-MSCs. When the cells grown on the substrates are coated with CDMs, YAP showed a higher

https://dx.doi.org/10.1021/acsami.0c05012
ACS Appl. Mater. Interfaces XXXX, XXX, XXX−XXX

enrichment into the nucleus (Figure 7A). Quantitative analysis (Figure 7B) indicated that the cell percentage with the YAP

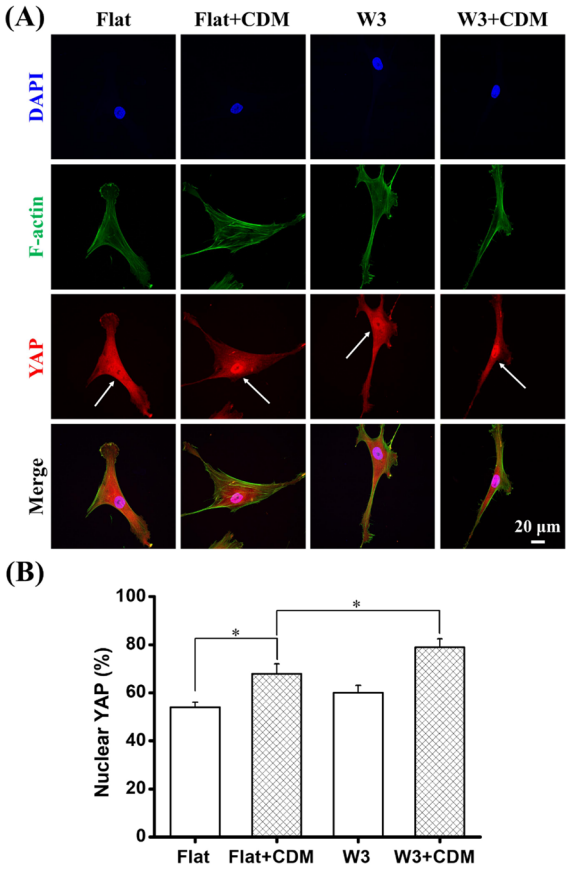

Figure 7. (A) Representative images of hBM-MSCs residing on different surfaces and the location of YAP after 24 h of seeding. Blue: nucleus, Green: F-actin, Red: YAP. The arrows refer to the YAP location. The scale bar is 20 μm. (B) The percentage of cells with YAP localized in the nucleus. Data are indicated as mean ± standard deviation (SD) ($n \geq 30$ cells, three independent experiments), and *$P < 0.01$.

located in the nucleus increased from 54 to 68% for Flat versus Flat + CDM and from 60 to 79% for W3 versus W3 + CDM, respectively. More interestingly, there is no significant difference between Flat and W3. However, for W3 + CDM, the percentage of nuclear positive cells for YAP is significantly higher than that for Flat + CDM, indicating that there is a synergistic influence of topography and CDMs on YAP localization. These findings indicate that the CDM facilitates the YAP translocation from the cytoplasm into the nucleus and that combining topography with CDMs enhances each other.

Considering the difference for YAP phosphorylation, the related mechanism was investigated to understand how the sensing of the cell of CDM + topography is related to the YAP localization in hBM-MSCs. Previously, the RhoA/ROCK/myosin-II, the major signaling pathway mediating the cytoskeletal contractility in nonmuscle mammalian cells, was shown to be important for regulating osteogenesis.[55] Intracellular tension can be characterized by phosphorylated myosin light chains (pMLCs). Immunofluorescence staining of pMLCs was performed for hBM-MSCs after culturing for 1 day. Representative immunofluorescence images of hBM-MSCs labeled with pMLCs are shown in Figure 8A. For

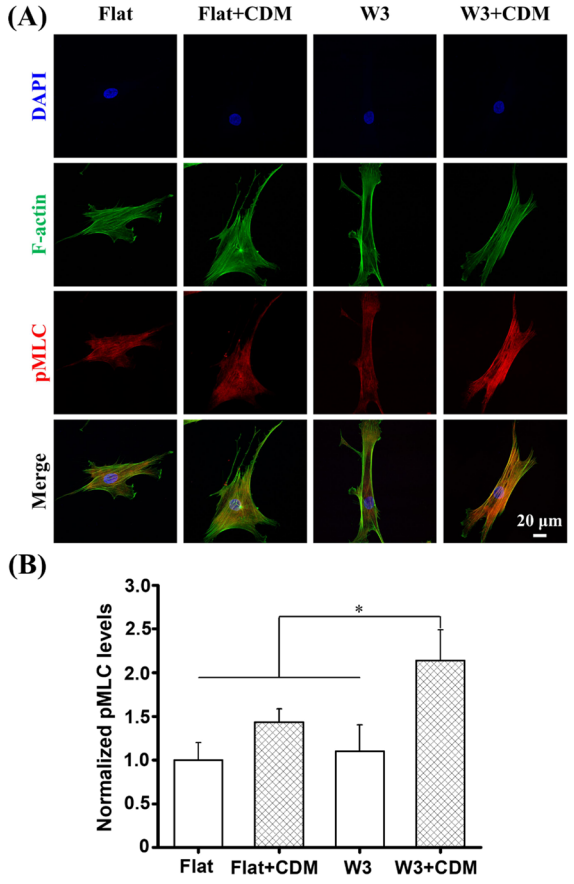

Figure 8. Fluorescence images of cell tension on the various substrates. (A) Representative images of single stem cells on the various substrates with and without CDMs in the growth medium cultured for 24 h. Nucleus (Blue), F-actin (Green), and pMLC (Red). The scale bar is 20 μm. (B) Integrated fluorescence intensity of pMLCs and that compared via normalization for the Flat substrate. Data are given as mean ± standard deviation (SD) ($n \geq 30$ cells, three independent experiments), and *$P < 0.05$.

cells grown on W3 + CDM it was found that these cells have a higher intensity of pMLCs in comparison to the other three groups. Quantification of the results indicates that the pMLC levels of cells on W3 + CDM were 2.1-, 1.46-, and 1.9-fold higher than those on the Flat, Flat + CDM, and W3, respectively (Figure 8B). It was found that there is no difference among the latter three substrates. These results indicate that the CDM layer has a great effect on cell tension or contractility but only when it is combined with the correct topography.

Vinculin is a marker protein for focal adhesion and interacts with F-actin to recruite actin filaments toward the sites of the focal adhesion.[56] Previously, it was shown that focal adhesion (FA) formation is related to the RhoA/ROCK signaling pathway by affecting the contractility of the cell. Also, it was found that more FAs are beneficial for osteogenesis.[57,58] To investigate the changes for vinculin expression of hBM-MSCs cultured on pristine topography versus CDM + topography, vinculin was stained and visualized by CLSM after culturing for 1 day. As shown in the immunofluorescence image (Figure 9A), vinculin spots with more well-defined dashlike structure were identified when the cells are grown on Flat + CDM and W3 + CDM, compared with Flat and W3, respectively, indicating that the CDM is able to enhance vinculin

https://dx.doi.org/10.1021/acsami.0c05012
ACS Appl. Mater. Interfaces XXXX, XXX, XXX−XXX

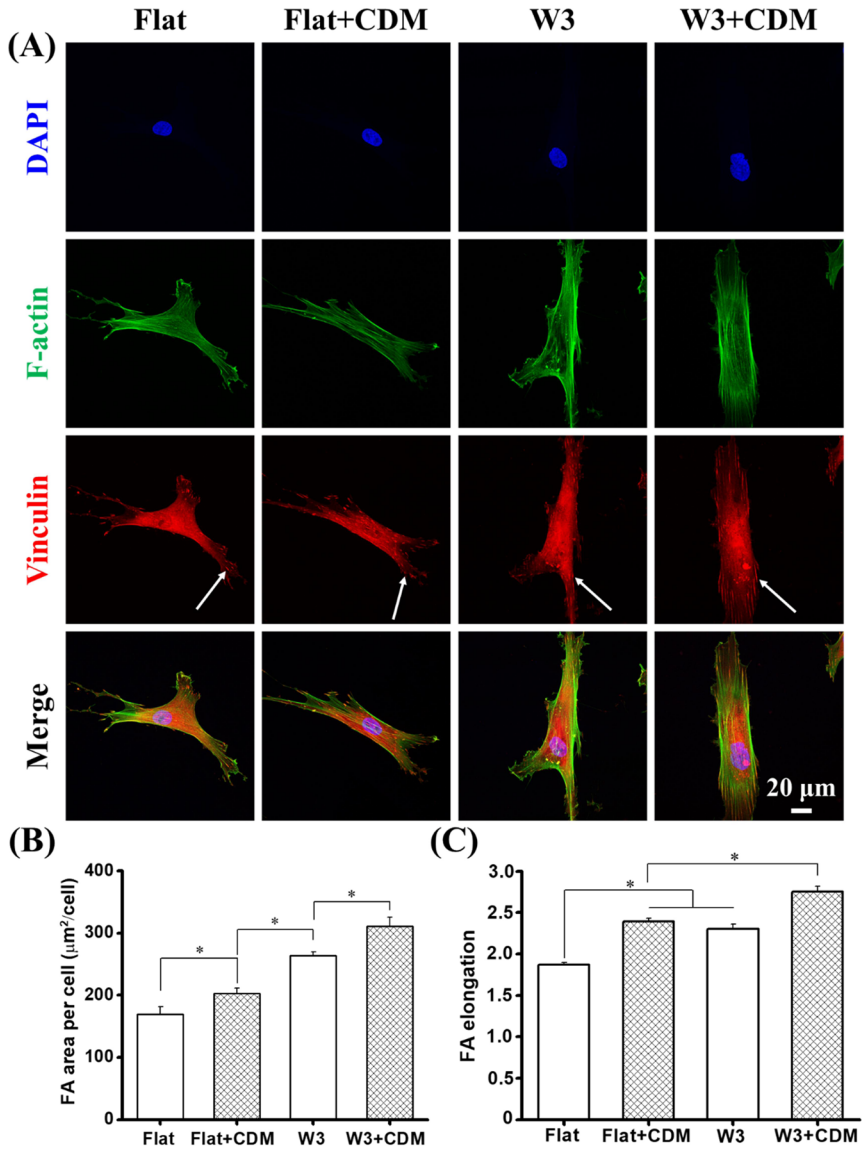

Figure 9. (A) Immunofluorescence staining of hBM-MSCs for vinculin after culturing for 1 day on various substrates. Blue: nucleus, Green: F-actin, and Red: vinculin. Grayscale image for vinculin is shown in Figure S4. The scale bar is 20 μm. Quantification of (B) FA area per cell and (C) FA elongation. The white arrows refer to the vinculin spots that are well-defined dashlike in structure. Data are displayed as mean ± standard deviation (SD) ($n \geq 30$ cells, three independent experiments), and $^*P < 0.05$.

expression. In comparison to the other three substrates, hBM-MSCs on W3 + CDM showed the highest expression. In general, micrometer-sized punctate structures are typically regarded as the mature FAs.[59] To gain more insights into the FA formation on various substrates, FA area per cell was quantified using an online Focal Adhesion Analysis Server[42] (Figure 9B). The FA area/cell progressively increased on CDM substrates, compared to the pristine topography substrates. FA area per cell for the cells cultured on W3 + CDM (310 μm^2) was much larger than that on Flat + CDM (202 μm^2), W3 (263 μm^2), and Flat (169 μm^2). As FA elongation is an indicator for the maturity,[60] the elongation was also quantified with the method mentioned above. It was observed that substrates deposited with the CDM exhibited increased FA elongation. As illustrated in Figure 9C, FA elongation for the cells grown on Flat + CDM was 2.39, higher than that on the Flat substrate (1.87), and there is a similar trend for W3 and W3 + CDM, varying from 2.3 to 2.75, suggesting that the CDM improves the maturity of FAs. Collectively, our findings suggest that the CDM on the wrinkle structure is able to facilitate the formation and elongation of FAs, strengthen the cell contractility, and activate translocation of more YAPs into the nucleus, leading to enhanced osteogenesis.

4. DISCUSSION

However, it is well established that both the CDM and topography are used to create a microenvironment that mimics the natural niche of stem cells and have a hight impact on cellular behaviors. There are relatively fewer studies that focus on their co-effect on osteogenesis of hBM-MSCs, and as far as we could identify, only one study performed by Zhao et al. elucidates that ECM sheets significanty increase calcium deposition of MSCs; however, their alignment does not seem to have an influence. In our study, PDMS-based anisotropic topography substrates with various wavelengths and ampli-

https://dx.doi.org/10.1021/acsami.0c05012
ACS Appl. Mater. Interfaces XXXX, XXX, XXX−XXX

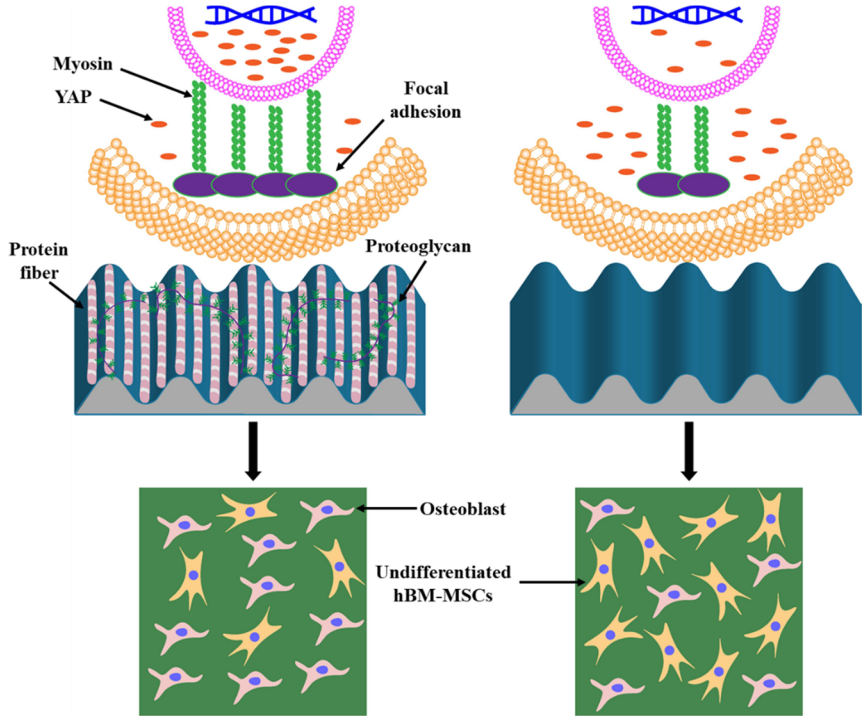

Figure 10. Schematic representation the effects of topography and Flat substrates coated with CDMs to direct osteogenic differentiation. Compared with the pristine W3 substrate, the wrinkle substrate coated with the CDM will enhance the formation and elongation of focal adhesions and strengthen cell contractility, resulting in the activation of YAP and translocation into the nucleus, therefore improving osteogenesis of hBM-MSCs.

tudes were prepared for studying the synergistic effect of CDMs and topography on osteogenesis. Furthermore, we found that the enhanced osteogenesis of hBM-MSCs on CDM−topography is partly mediated by focal adhesion, cytoskeletal contractility, and YAP signaling activation.

The topographies used in this study relate to the natural ECM in the sense that they have a fiberlike morphology rather than the shape-edged gratings that are often used. Furthermore, the W0.5 topography represents the nanoscale features found in the ECM in vivo, while W3 and W10 represent the microscale features. Previously, these patterns were found to influence hBM-MSCs with respect to osteogenic differentiation.[14] Therefore, in this study, we choose these patterns to further elucidate the synergism between CDMs and topography on osteogenic differentiation. For the preparation of extracellular matrices, some previous studies used the ECM scaffolds derived from tissues such as muscle[61] and cartilage.[62] Compared with tissues, cultured cells have several advantages, for example, possibility of mixing ECMs harvested from different types of cells and the potential of originating from autologous cells to provide autologous ECM scaffolds to avoid the undesired host responses.[36] After decellularization, the fibroblast-derived ECM maintains a good morphology and network structure (Figure 3A,B), and the orientation distribution of ECM fiber is dependent on the dimension of the wrinkle (Figure 3C,D), indicating strong correlation with the fibroblast response to the wrinkle topography. Although the main type of the matrix components remained the same, growth factor secretion (e.g., *TGF-β1, bFGF,* and *VEGF*) by cells was not considered here but could have an altered composition and be confined within the matrix even after the extensive washing steps. Furthermore, we also demonstrate that there is an important influence of CDMs on the cell orientation, the cell area, and the aspect ratio (Figure 4).

Our results agree well with results from previous studies[61] in which Cho et al. demonstrated that topographical and derived ECMs have a synergistic effect on myogenic differentiation and maturation. Furthermore, we found that there is a varied degree of OPN expression and mineralization on different wrinkle size substrates decorated with CDMs, which is inconsistent with the findings of Zhao and co-workers.[34] In their study, they cultured stem cells on Flat and nanopatterned substrates of 130 nm in depth and 350 nm in width, deposited with fibroblast-derived ECMs, and found that the aligned topography did not influence the osteogenic activity. However, they did not vary the parameter of the topography, therefore overseeing certain possible positive correlations as we present here. With the deposition of the CDM, the fibers also align to some degree to the topography due to the alignment of the fibroblasts that deposited it. From the various results, it can be concluded that the synergy is not due to simply introducing the biochemical nature of the CDM or its alignment. Comparing Flat with and without CDMs, there is no enhancement in osteogenenis. Therefore, only adding the biochemical nature does not provide substantial stimuli. When aligning the CDM as seen on the W10 substrates, also the alignment with the biochemical nature of the CDM does not enhance differentiation. Only for W0.5 and W3 with CDMs, a synergistic effect is observed despite the difference in CDM alignment between the two substrates, while for OPN expression, both these topographies with CDMs display a synergistic effect; considering the final functional state, namely, mineralization, the enhancement is more prominent for W3 + CDM. That is, the difference for W0.5 is less efficient than that for W3, which might be due to the addition of the CDM,

https://dx.doi.org/10.1021/acsami.0c05012
ACS Appl. Mater. Interfaces XXXX, XXX, XXX−XXX

thereby masking to some degree the topographical stimulation of the cell, which is still clearly visible for the W3 + CDM (Figure 2). We recently showed that topographies, both the amplitude and wavelength, play an important role[63] but overcrowding the topography too much will certainly make the stimulus less pronounced.

Until now, although some researchers have elucidated that for proliferation, migration, and differentiation on topography[64] and stiffness[65] of the substrate, YAP-dependent mechanotransduction is required, few studies investigated the mechanotransduction of cells cultured on CDMs. Park et al.[28] identified the mechanotransduction of human pluripotent stem cells (hPSCs) cultured on fibroblast-derived matrices (FDMs) with decellularization, to elucidate cell adhesion, proliferation, migration, and pluripotency. Their results indicate that stiffness of FDMs is a dominant influence in mediating hPSC plasticity. Recently, Yang and co-workers[66] found that increasing the density of ECM ligands (Fn, Col I, Col IV, and laminin) alone can trigger nuclear translocation of YAP without changing substrate stiffness and further showed that altering the type of ECM modulates hMSC osteogenic differentiation without altering the stiffness of the substrate. Therefore, their findings highlight the important role of ECMs in modulating mechanotransduction and differentiation of stem cells. Furthermore, Besenbacher et al.[67] found that the adsorption of Fn (a major component of the ECM) facilitates focal adhesion formation as compared to the uncoated surface, which is consistent with our current findings (Figure 9). In our study, we not only showed that the combination of CDMs and topography synergistically enhances osteogenic differentiation (Figure 5 and 6), but also investigated the related proteins involved in the process of mechanotransduction. We demonstrated that for the substrate W3 + CDM, the higher expression of OPN and mineralization might be because of the increased formation and elongation of FAs (Figure 9), stronger cytoskeleton contractility (Figure 8), and more YAP translocated into the nucleus (Figure 7), leading to the expression of the related gene in osteogenic differentiation. The potential mechanism for the improved capacity of osteogenesis on W3 + CDM mediated by focal adhesion, cytoskeletal tension, and the YAP signaling pathway is illustrated in Figure 10. As there are other pathways involved in the osteogenesis process, for example, the mitogen-activated protein kinase (MAPK) pathway[68] and focal adhesion kinase/MAPK and integrin linked kinase/β-Catenin pathways.[69] Therefore, further investigations are needed to fully identify the mechanisms involved in the osteogenic differentiation process stimulated by CDMs and topography.

5. CONCLUSIONS

In this study, we prepared an anisotropic wrinkle substrate with different wavelengths and amplitudes and harvested the cell-derived extracellular matrix to investigate the synergistic effect on the morphology and osteogenesis of hBM-MSCs. We demonstrate that substrates decorated with CDMs have a significant impact on cell area and orientation distribution. Moreover, compared to Flat, Flat + CDM, W3, and W3 + CDM significantly facilitate the fate of hBM-MSCs toward the osteogenic lineage. In addition, this process is connected to a higher percentage of cells with YAP localized within the nucleus, stronger cell tension, and greater formation of focal adhesions. Taken together, this study displays the importance of the ECM in cellular fate decisions, and the CDM is able to provide useful approaches to study the interaction between the natural matrix and stem cells, which could facilitate viable applications in tissue engineering and regenerative medicine.

■ ASSOCIATED CONTENT

Supporting Information

The Supporting Information is available free of charge at https://pubs.acs.org/doi/10.1021/acsami.0c05012.

Figure S1. Representative fluorescence images of fibroblasts grown on pristine topography for 1 and 10 days. Figure S2. Quantification of density of hBM-MSCs seeded onto pristine wrinkle surfaces and substrates coated with CDMs after 1 and 14 days. Figure S3. Integrated fluorescence intensity of Fn normalized by the mean values of the Flat substrate. Figure S4. Grayscale image for vinculin staining (PDF)

■ AUTHOR INFORMATION

Corresponding Authors

Liangliang Yang − *Department of Biomedical Engineering-FB40, University of Groningen, University Medical Center Groningen, Groningen, 9713 Groningen, The Netherlands; W.J. Kolff Institute for Biomedical Engineering and Materials Science-FB41, Groningen, University of Groningen, University Medical Center Groningen, 9713 Groningen, The Netherlands;* Email: l.yang@umcg.nl

Patrick van Rijn − *Department of Biomedical Engineering-FB40, University of Groningen, University Medical Center Groningen, Groningen, 9713 Groningen, The Netherlands; W.J. Kolff Institute for Biomedical Engineering and Materials Science-FB41, Groningen, University of Groningen, University Medical Center Groningen, 9713 Groningen, The Netherlands;* orcid.org/0000-0002-2208-5725; Email: p.van.rijn@umcg.nl

Author

Lu Ge − *Department of Biomedical Engineering-FB40, University of Groningen, University Medical Center Groningen, Groningen, 9713 Groningen, The Netherlands; W.J. Kolff Institute for Biomedical Engineering and Materials Science-FB41, Groningen, University of Groningen, University Medical Center Groningen, 9713 Groningen, The Netherlands;* orcid.org/0000-0002-5782-4823

Complete contact information is available at: https://pubs.acs.org/10.1021/acsami.0c05012

Notes

The authors declare the following competing financial interest(s): P.v.R. also is co-founder, scientific advisor, and share-holder of BiomACS BV, a biomedical oriented screening company. The authors declare no other competing interests.

■ ACKNOWLEDGMENTS

The authors are very grateful for financial support from the China Scholarship Council (no. 201608310113 and 201707720058) and the UMCG Microscopy and Imaging Center (UMIC) (NWO-grant 40-00506-98-9021). We thank Klaas Sjollema for assistance with the TissueFaxs microscope.

REFERENCES

(1) Humphrey, J. D.; Dufresne, E. R.; Schwartz, M. A. Mechanotransduction and Extracellular Matrix Homeostasis. *Nat. Rev. Mol. Cell Biol.* **2014**, *15*, 802−812.

(2) Murphy, W. L.; McDevitt, T. C.; Engler, A. J. Materials as Stem Cell Regulators. *Nat. Mater.* **2014**, *13*, 547−557.

(3) Lutolf, M. P.; Gilbert, P. M.; Blau, H. M. Designing Materials to Direct Stem-Cell Fate. *Nature* **2009**, *462*, 433−441.

(4) Ko, E.; Yu, S. J.; Pagan-Diaz, G. J.; Mahmassani, Z.; Boppart, M. D.; Im, S. G.; Bashir, R.; Kong, H. Matrix Topography Regulates Synaptic Transmission at the Neuromuscular Junction. *Adv. Sci.* **2019**, *6*, 1801521−1801531.

(5) Poudineh, M.; Wang, Z.; Labib, M.; Ahmadi, M.; Zhang, L.; Das, J.; Ahmed, S. U.; Angers, S.; Kelley, S. O. Three-Dimensional Nanostructured Architectures Enable Efficient Neural Differentiation of Mesenchymal Stem Cells via Mechanotransduction. *Nano Lett.* **2018**, *18*, 7188−7193.

(6) Dalby, M. J.; Gadegaard, N.; Oreffo, R. O. C. Harnessing Nanotopography and Integrin-Matrix Interactions to Influence Stem Cell Fate. *Nat. Mater.* **2014**, *13*, 558−569.

(7) Baek, J.; Jung, W.-B.; Cho, Y.; Lee, E.; Yun, G.-T.; Cho, S.-Y.; Jung, H.-T.; Im, S. G. Facile Fabrication of High-Definition Hierarchical Wrinkle Structures for Investigating the Geometry-Sensitive Fate Commitment of Human Neural Stem Cells. *ACS Appl. Mater. Interfaces* **2019**, *11*, 17247−17255.

(8) Zhang, X.; Cui, X.; Wang, D.; Wang, S.; Liu, Z.; Zhao, G.; Zhang, Y.; Li, Z.; Wang, Z. L.; Li, L. Piezoelectric Nanotopography Induced Neuron-Like Differentiation of Stem Cells. *Adv. Funct. Mater.* **2019**, *29*, 1900372−1900381.

(9) Kim, J.; Kim, H. N.; Lim, K. T.; Kim, Y.; Pandey, S.; Garg, P.; Choung, Y. H.; Choung, P. H.; Suh, K. Y.; Chung, J. H. Synergistic Effects of Nanotopography and Co-Culture with Endothelial Cells on Osteogenesis of Mesenchymal Stem Cells. *Biomaterials* **2013**, *34*, 7257−7268.

(10) Dalby, M. J.; Riehle, M. O.; Johnstone, H.; Affrossman, S.; Curtis, A. S. Investigating the Limits of Filopodial Sensing: A Brief Report Using SEM to Image the Interaction between 10 Nm High Nano-topography and Fibroblast Filopodia. *Cell Biol. Int.* **2004**, *28*, 229−236.

(11) Zhou, Q.; Castañeda Ocampo, O.; Guimarães, C. F.; Kühn, P. T.; Van Kooten, T. G.; van Rijn, P. Screening Platform for Cell Contact Guidance Based on Inorganic Biomaterial Micro/Nanotopographical Gradients. *ACS Appl. Mater. Interfaces* **2017**, *9*, 31433−31445.

(12) Abagnale, G.; Sechi, A.; Steger, M.; Zhou, Q.; Kuo, C. C.; Aydin, G.; Schalla, C.; Müller-Newen, G.; Zenke, M.; Costa, I. G.; van Rijn, P.; Gillner, A.; Wagner, W. Surface Topography Guides Morphology and Spatial Patterning of Induced Pluripotent Stem Cell Colonies. *Stem Cell Rep.* **2017**, *9*, 654−666.

(13) Liguori, G. R.; Zhou, Q.; Liguori, T. T. A.; Barros, G. G.; Kühn, P. T.; Moreira, L. F. P.; van Rijn, P.; Harmsen, M. C. Directional Topography Influences Adipose Mesenchymal Stromal Cell Plasticity: Prospects for Tissue Engineering and Fibrosis. *Stem Cells Int.* **2019**, *2019*, 1−14.

(14) Yang, L.; Gao, Q.; Ge, L.; Zhou, Q.; Warszawik, E. M.; Bron, R.; Lai, K. W. C.; van Rijn, P. Topography Induced Stiffness Alteration of Stem Cells Influences Osteogenic Differentiation. *Biomater. Sci.* **2020**, *8*, 2638−2652.

(15) Yang, L.; Jurczak, K. M.; Ge, L.; van Rijn, P. High Throughput Screening and Hierarchical Topography-Mediated Neural Differentiation of Mesenchymal Stem Cells. *Adv. Healthcare Mater.* **2020**, 2000117.

(16) Yang, L.; Ge, L.; Zhou, Q.; Mokabber, T.; Pei, Y.; Bron, R.; van Rijn, P. Biomimetic Multiscale Hierarchical Topography Enhances Osteogenic Differentiation of Human Mesenchymal Stem Cells. *Adv. Mater. Interfaces* **2020**, 2000385. In press

(17) Ge, L.; Yang, L.; Bron, R.; Burgess, J. K.; van Rijn, P. Topography-Mediated Fibroblast Cell Migration Is Influenced by Direction, Wavelength, and Amplitude. *ACS Appl. Bio Mater.* **2020**, *3*, 2104−2116.

(18) Lutolf, M. P.; Hubbell, J. A. Synthetic Biomaterials as Instructive Extracellular Microenvironments for Morphogenesis in Tissue Engineering. *Nat. Biotechnol.* **2005**, *23*, 47−55.

(19) Brown, J. H.; Das, P.; DiVito, M. D.; Ivancic, D.; Poh Tan, L.; Wertheim, J. A. Nanofibrous PLGA Electrospun Scaffolds Modified with Type I Collagen Influence Hepatocyte Function and Support Viability In Vitro. *Acta Biomater.* **2018**, *73*, 217−227.

(20) Rico, P.; Mnatsakanyan, H.; Dalby, M. J.; Salmerón-Sánchez, M. Material-Driven Fibronectin Assembly Promotes Maintenance of Mesenchymal Stem Cell Phenotypes. *Adv. Funct. Mater.* **2016**, *26*, 6563−6573.

(21) Lee, S.; Stanton, A. E.; Tong, X.; Yang, F. Hydrogels with Enhanced Protein Conjugation Efficiency Reveal Stiffness-Induced YAP Localization in Stem Cells Depends on Biochemical Cues. *Biomaterials* **2019**, *202*, 26−34.

(22) Gehlen, D. B.; De Lencastre Novaes, L. C.; Long, W.; Ruff, A. J.; Jakob, F.; Haraszti, T.; Chandorkar, Y.; Yang, L.; van Rijn, P.; Schwaneberg, U.; de Laporte, L. Rapid and Robust Coating Method to Render Polydimethylsiloxane Surfaces Cell-Adhesive. *ACS Appl. Mater. Interfaces* **2019**, *11*, 41091−41099.

(23) Silantyeva, E. A.; Nasir, W.; Carpenter, J.; Manahan, O.; Becker, M. L.; Willits, R. K. Accelerated Neural Differentiation of Mouse Embryonic Stem Cells on Aligned GYIGSR-Functionalized Nanofibers. *Acta Biomater.* **2018**, *75*, 129−139.

(24) Cheong, H.; Kim, J.; Kim, B. J.; Kim, E.; Park, H. Y.; Choi, B. H.; Joo, K. I.; Cho, M.-L.; Rhie, J. W.; Lee, J. I.; Cha, H. J. Multi-Dimensional Bioinspired Tactics Using an Engineered Mussel Protein Glue-Based Nanofiber Conduit for Accelerated Functional Nerve Regeneration. *Acta Biomater.* **2019**, *90*, 87−99.

(25) Zhu, M.; Lin, S.; Sun, Y.; Feng, Q.; Li, G.; Bian, L. Hydrogels Functionalized with N-Cadherin Mimetic Peptide Enhance Osteogenesis of HMSCs by Emulating the Osteogenic Niche. *Biomaterials* **2016**, *77*, 44−52.

(26) Li, J.; Di Russo, J.; Hua, X.; Chu, Z.; Spatz, J. P.; Wei, Q. Surface Immobilized E-Cadherin Mimetic Peptide Regulates the Adhesion and Clustering of Epithelial Cells. *Adv. Healthcare Mater.* **2019**, *8*, No. e1801384.

(27) Yang, Y.; Lin, H.; Shen, H.; Wang, B.; Lei, G.; Tuan, R. S. Mesenchymal Stem Cell-Derived Extracellular Matrix Enhances Chondrogenic Phenotype of and Cartilage Formation by Encapsulated Chondrocytes in Vitro and in Vivo. *Acta Biomater.* **2018**, *69*, 71−82.

(28) Kim, I. G.; Gil, C. H.; Seo, J.; Park, S. J.; Subbiah, R.; Jung, T. H.; Kim, J. S.; Jeong, Y. H.; Chung, H. M.; Lee, J. H.; Lee, M. R.; Hwan Moon, S.; Park, K. Mechanotransduction of Human Pluripotent Stem Cells Cultivated on Tunable Cell-Derived Extracellular Matrix. *Biomaterials* **2018**, *150*, 100−111.

(29) Discher, D. E.; Mooney, D. J.; Zandstra, P. W. Growth Factors, Matrices, and Forces Combine and Control Stem Cells. *Science* **2009**, *324*, 1673−1677.

(30) Järveläinen, H.; Sainio, A.; Koulu, M.; Wight, T. N.; Penttinen, R. Extracellular Matrix Molecules: Potential Targets in Pharmacotherapy. *Pharmacol. Rev.* **2009**, *61*, 198−223.

(31) Eyckmans, J.; Boudou, T.; Yu, X.; Chen, C. S. A Hitchhiker's Guide to Mechanobiology. *Dev. Cell* **2011**, *21*, 35−47.

(32) Harvestine, J. N.; Orbay, H.; Chen, J. Y.; Sahar, D. E.; Leach, J. K. Cell-Secreted Extracellular Matrix, Independent of Cell Source, Promotes the Osteogenic Differentiation of Human Stromal Vascular Fraction. *J. Mater. Chem. B* **2018**, *6*, 4104−4115.

(33) Sart, S.; Yan, Y.; Lochner, E.; Zeng, C.; Ma, T.; Li, Y. Crosslinking of Extracellular Matrix Scaffolds Derived from Pluripotent Stem Cell Aggregates Modulates Neural Differentiation. *Acta Biomater.* **2016**, *30*, 222−232.

(34) Xing, Q.; Qian, Z.; Kannan, B.; Tahtinen, M.; Zhao, F. Osteogenic Differentiation Evaluation of an Engineered Extracellular Matrix Based Tissue Sheet for Potential Periosteum Replacement. *ACS Appl. Mater. Interfaces* **2015**, *7*, 23239−23247.

https://dx.doi.org/10.1021/acsami.0c05012
ACS Appl. Mater. Interfaces XXXX, XXX, XXX−XXX

(35) Xing, Q.; Vogt, C.; Leong, K. W.; Zhao, F. Highly Aligned Nanofibrous Scaffold Derived from Decellularized Human Fibroblasts. *Adv. Funct. Mater.* **2014**, *24*, 3027−3035.
(36) Lu, H.; Hoshiba, T.; Kawazoe, N.; Koda, I.; Song, M.; Chen, G. Cultured Cell-Derived Extracellular Matrix Scaffolds for Tissue Engineering. *Biomaterials* **2011**, *32*, 9658−9666.
(37) Cai, R.; Nakamoto, T.; Hoshiba, T.; Kawazoe, N.; Chen, G. Matrices Secreted during Simultaneous Osteogenesis and Adipogenesis of Mesenchymal Stem Cells Affect Stem Cells Differentiation. *Acta Biomater.* **2016**, *35*, 185−193.
(38) Kaukonen, R.; Jacquemet, G.; Hamidi, H.; Ivaska, J. Cell-Derived Matrices for Studying Cell Proliferation and Directional Migration in a Complex 3D Microenvironment. *Nat. Protoc.* **2017**, *12*, 2376−2390.
(39) Ahlfors, J. E. W.; Billiar, K. L. Biomechanical and Biochemical Characteristics of a Human Fibroblast-Produced and Remodeled Matrix. *Biomaterials* **2007**, *28*, 2183−2191.
(40) Lin, H.; Yang, G.; Tan, J.; Tuan, R. S. Influence of Decellularized Matrix Derived from Human Mesenchymal Stem Cells on Their Proliferation, Migration and Multi-Lineage Differentiation Potential. *Biomaterials* **2012**, *33*, 4480−4489.
(41) Ragelle, H.; Naba, A.; Larson, B. L.; Zhou, F.; Prijić, M.; Whittaker, C. A.; Del Rosario, A.; Langer, R.; Hynes, R. O.; Anderson, D. G. Comprehensive Proteomic Characterization of Stem Cell-Derived Extracellular Matrices. *Biomaterials* **2017**, *128*, 147−159.
(42) Berginski, M. E.; Gomez, S. M. The Focal Adhesion Analysis Server: A Web Tool for Analyzing Focal Adhesion Dynamics. *F1000Res* **2013**, *2*, 68−71.
(43) Liu, X.; Liu, R.; Cao, B.; Ye, K.; Li, S.; Gu, Y.; Pan, Z.; Ding, J. Subcellular Cell Geometry on Micropillars Regulates Stem Cell Differentiation. *Biomaterials* **2016**, *111*, 27−39.
(44) Zhang, K.; Zheng, H.; Liang, S.; Gao, C. Aligned PLLA Nanofibrous Scaffolds Coated with Graphene Oxide for Promoting Neural Cell Growth. *Acta Biomater.* **2016**, *37*, 131−142.
(45) Charest, J. L.; Eliason, M. T.; García, A. J.; King, W. P. Combined Microscale Mechanical Topography and Chemical Patterns on Polymer Cell Culture Substrates. *Biomaterials* **2006**, *27*, 2487−2494.
(46) Takahashi, H.; Shimizu, T.; Nakayama, M.; Yamato, M.; Okano, T. Anisotropic Cellular Network Formation in Engineered Muscle Tissue through the Self-Organization of Neurons and Endothelial Cells. *Adv. Healthcare Mater.* **2015**, *4*, 356−360.
(47) Charest, J. L.; García, A. J.; King, W. P. Myoblast Alignment and Differentiation on Cell Culture Substrates with Microscale Topography and Model Chemistries. *Biomaterials* **2007**, *28*, 2202−2210.
(48) Eid, A. A.; Hussein, K. A.; Niu, L.; Li, G.; Watanabe, I.; Al-Shabrawey, M.; Pashley, D. H.; Tay, F. R. Effects of Tricalcium Silicate Cements on Osteogenic Differentiation of Human Bone Marrow-Derived Mesenchymal Stem Cells in Vitro. *Acta Biomater.* **2014**, *10*, 3327−3334.
(49) Qiu, J.; Li, J.; Wang, S.; Ma, B.; Zhang, S.; Guo, W.; Zhang, X.; Tang, W.; Sang, Y.; Liu, H. TiO2 Nanorod Array Constructed Nanotopography for Regulation of Mesenchymal Stem Cells Fate and the Realization of Location-Committed Stem Cell Differentiation. *Small* **2016**, *12*, 1770−1778.
(50) Stanton, A. E.; Tong, X.; Lee, S.; Yang, F. Biochemical Ligand Density Regulates Yes-Associated Protein Translocation in Stem Cells through Cytoskeletal Tension and Integrins. *ACS Appl. Mater. Interfaces* **2019**, *11*, 8849−8857.
(51) Han, P.; Frith, J. E.; Gomez, G. A.; Yap, A. S.; O'Neill, G. M.; Cooper-White, J. J. Five Piconewtons: The Difference between Osteogenic and Adipogenic Fate Choice in Human Mesenchymal Stem Cells. *ACS Nano* **2019**, *13*, 11129−11143.
(52) Xue, X.; Hong, X.; Li, Z.; Deng, C. X.; Fu, J. Acoustic Tweezing Cytometry Enhances Osteogenesis of Human Mesenchymal Stem Cells through Cytoskeletal Contractility and YAP Activation. *Biomaterials* **2017**, *134*, 22−30.
(53) Li, L.; Yang, S.; Xu, L.; Li, Y.; Fu, Y.; Zhang, H.; Song, J. Nanotopography on Titanium Promotes Osteogenesis via Autophagy-Mediated Signaling between YAP and β-Catenin. *Acta Biomater.* **2019**, *96*, 674−685.
(54) Dupont, S.; Morsut, L.; Aragona, M.; Enzo, E.; Giulitti, S.; Cordenonsi, M.; Zanconato, F.; Le Digabel, J.; Forcato, M.; Bicciato, S.; Elvassore, N.; Piccolo, S. Role of YAP/TAZ in Mechanotransduction. *Nature* **2011**, *474*, 179−183.
(55) Khatiwala, C. B.; Kim, P. D.; Peyton, S. R.; Putnam, A. J. ECM Compliance Regulates Osteogenesis by Influencing MAPK Signaling Downstream of RhoA and ROCK. *J. Bone Miner. Res.* **2009**, *24*, 886−898.
(56) Golji, J.; Mofrad, M. R. K. The Interaction of Vinculin with Actin. *PLoS Comput. Biol.* **2013**, *9*, No. e1002995.
(57) Lauria, I.; Kramer, M.; Schröder, T.; Kant, S.; Hausmann, A.; Böke, F.; Leube, R.; Telle, R.; Fischer, H. Inkjet Printed Periodical Micropatterns Made of Inert Alumina Ceramics Induce Contact Guidance and Stimulate Osteogenic Differentiation of Mesenchymal Stromal Cells. *Acta Biomater.* **2016**, *44*, 85−96.
(58) Zhou, C.; Zhang, D.; Zou, J.; Li, X.; Zou, S.; Xie, J. Substrate Compliance Directs the Osteogenic Lineages of Stem Cells from the Human Apical Papilla via the Processes of Mechanosensing and Mechanotransduction. *ACS Appl. Mater. Interfaces* **2019**, *11*, 26448−26459.
(59) Turner, C. E. Paxillin and Focal Adhesion Signalling. *Nat. Cell Biol.* **2000**, *2*, E231−E236.
(60) Prager-Khoutorsky, M.; Lichtenstein, A.; Krishnan, R.; Rajendran, K.; Mayo, A.; Kam, Z.; Geiger, B.; Bershadsky, A. D. Fibroblast Polarization Is a Matrix-Rigidity-Dependent Process Controlled by Focal Adhesion Mechanosensing. *Nat. Cell Biol.* **2011**, *13*, 1457−1465.
(61) Choi, Y.-J.; Park, S. J.; Yi, H.-G.; Lee, H.; Kim, D. S.; Cho, D.-W. Muscle-Derived Extracellular Matrix on Sinusoidal Wavy Surfaces Synergistically Promotes Myogenic Differentiation and Maturation. *J. Mater. Chem. B* **2018**, *6*, 5530−5539.
(62) Cheng, N.-C.; Estes, B. T.; Young, T.-H.; Guilak, F. Genipin-Crosslinked Cartilage-Derived Matrix as a Scaffold for Human Adipose-Derived Stem Cell Chondrogenesis. *Tissue Eng. Part A* **2013**, *19*, 484−496.
(63) Yang, L.; Ge, L.; Zhou, Q.; Jurczak, K.; van Rijn, P. Decoupling the Amplitude and Wavelength of Anisotropic Topography and the Influence on Osteogenic Differentiation of Mesenchymal Stem Cells Using a High-Throughput Screening Approach. *ACS Appl. Bio Mater.* **2020**, DOI: 10.1021/acsabm.0c00330. In press
(64) Mascharak, S.; Benitez, P. L.; Proctor, A. C.; Madl, C. M.; Hu, K. H.; Dewi, R. E.; Butte, M. J.; Heilshorn, S. C. YAP-Dependent Mechanotransduction Is Required for Proliferation and Migration on Native-like Substrate Topography. *Biomaterials* **2017**, *115*, 155−166.
(65) Chu, G.; Yuan, Z.; Zhu, C.; Zhou, P.; Wang, H.; Zhang, W.; Cai, Y.; Zhu, X.; Yang, H.; Li, B. Substrate Stiffness- and Topography-Dependent Differentiation of Annulus Fibrosus-Derived Stem Cells Is Regulated by Yes-Associated Protein. *Acta Biomater.* **2019**, *92*, 254−264.
(66) Stanton, A. E.; Tong, X.; Yang, F. Extracellular Matrix Type Modulates Mechanotransduction of Stem Cells. *Acta Biomater.* **2019**, *96*, 310−320.
(67) Dolatshahi-Pirouz, A.; Jensen, T.; Kraft, D. C.; Foss, M.; Kingshott, P.; Hansen, J. L.; Larsen, A. N.; Chevallier, J.; Besenbacher, F. Fibronectin Adsorption, Cell Adhesion, and Proliferation on Nanostructured Tantalum Surfaces. *ACS Nano* **2010**, *4*, 2874−2882.
(68) Wang, Q.; Chen, B.; Cao, M.; Sun, J.; Wu, H.; Zhao, P.; Xing, J.; Yang, Y.; Zhang, X.; Ji, M.; Gu, N. Response of MAPK Pathway to Iron Oxide Nanoparticles in Vitro Treatment Promotes Osteogenic Differentiation of HBMSCs. *Biomaterials* **2016**, *86*, 11−20.
(69) Niu, H.; Lin, D.; Tang, W.; Ma, Y.; Duan, B.; Yuan, Y.; Liu, C. Surface Topography Regulates Osteogenic Differentiation of MSCs via Crosstalk between FAK/MAPK and ILK/β-Catenin Pathways in a Hierarchically Porous Environment. *ACS Biomater. Sci. Eng.* **2017**, *3*, 3161−3175.

https://dx.doi.org/10.1021/acsami.0c05012
ACS Appl. Mater. Interfaces XXXX, XXX, XXX−XXX